electronics

MDPI

Article

A New Method of Conductor Galloping Monitoring Using the Target Detection of Infrared Source

Yufeng Gao [1,*], Jun Yang [1], Ke Zhang [2], Huaizhen Peng [3], Yin Wang [3], Na Xia [3] and Gang Yao [1]

[1] Hangzhou Power Supply Company, State Grid Zhejiang Electric Power Co., Ltd., Hangzhou 310000, China; kety@zju.edu.cn (J.Y.); zmanda97@163.com (G.Y.)
[2] State Grid Electric Power Research Institute Co., Ltd., Hefei 230088, China; 13637052098@163.com
[3] School of Computer Science and Information Engineering, Hefei University of Technology, Hefei 230601, China; 2018110976@mail.hfut.edu.cn (H.P.); wangyin950203@gmail.com (Y.W.); xiananawo@hfut.edu.cn (N.X.)
* Correspondence: aimer_17@163.com; Tel.: +86-136-6669-6055

Abstract: Because the galloping of iced conductors is one of the main disasters in the State Grid, resulting in huge economic and property losses every year, the research on relevant monitoring methods is of great significance. The existing galloping monitoring technology is mainly based on the contact detection method, which presents potential electrical hazards and power supply problems. In this paper, a conductor galloping monitoring method based on the target detection of infrared sources is put forward to overcome the shortcomings of existing methods. In other words, an infrared source label is installed on the conductor spacer, high-definition night vision infrared cameras are installed on electric power towers to take video of the infrared source labels, and the characteristic amplitude of conductor galloping is calculated by an image recognition and tracking algorithm. The practical application results indicate that the method has the advantages of non-contact detection, safety and reliability, and high detection accuracy.

Keywords: infrared source; image recognition; meteorological; low power consumption

Citation: Gao, Y.; Yang, J.; Zhang, K.; Peng, H.; Wang, Y.; Xia, N.; Yao, G. A New Method of Conductor Galloping Monitoring Using the Target Detection of Infrared Source. *Electronics* **2022**, *11*, 1207. https://doi.org/10.3390/electronics11081207

Academic Editors: Pierluigi Siano, Hassan Haes Alhelou and Amer Al-Hinai

Received: 9 March 2022
Accepted: 8 April 2022
Published: 11 April 2022

1. Introduction

In recent years, the construction of power transmission lines across China has become faster and faster, and the requirements for lean power transmission management have become more demanding. As of the end of 2019, the combined length of 110 (66) kV and higher transmission lines was 1.0934 million km, and the line length of UHV projects in operation was over 38,000 km. The number of incidents of wire dancing has been is increasing year by year. Since 1957, more than 1500 galloping accidents have been recorded in China, and transmission lines of different levels from 10 kV to 1100 kV have been affected, resulting in economic losses in the tens of billions of RMB.

Conductor galloping refers to a type of low-frequency, large-amplitude self-excited vibration caused by eccentric icing of transmission line conductors and wind excitation. It can cause serious accidents such as line tripping, damage to armor clamps and insulators, broken conductor strands or broken lines, damage to electric power towers, damage to foundations, and even tower collapse. It can be seen that it is a serious disaster that endangers the safe and stable operation of transmission lines [1,2]. Therefore, it is of great significance to study effective monitoring techniques for conductor galloping.

2. Related Works

It is difficult to measure the trajectory of conductor galloping with existing models. Several scholars have studied the trajectories of conductor galloping in an attempt to find models that can analyze the trajectories and predict the amplitude of conductor galloping [3–9], . Some scholars have applied UAV target tracking and detection to conductor

galloping monitoring [10]. However, although this method has high monitoring accuracy, it cannot achieve all-weather automatic monitoring, and the cost is high. At present, there are two main methods to monitor conductor galloping. One type of non-contact monitoring of conductor galloping is achieved through video capture images and image analysis modules. By installing cameras on poles or towers, the conductors are photographed or videoed, and then the data is transmitted back to the monitoring center. At the monitoring end, the motion state of the conductor is observed manually to judge whether it is galloping or not. This method is intuitive and can qualitatively judge the galloping state, but it depends on manual work and cannot be used for automatic detection, let alone providing warnings in advance.

As a result, automated systems have gradually emerged that model and analyze the images sent back to the monitoring end and set up early warning mechanisms. In reference [11], a transmission conductor video monitoring device was used to obtain video information on conductor galloping. Multiple frames of continuous images taken from the transmission conductor galloping video were used to create contour feature templates by selecting the conductor spacer bars as the tracking targets, and by matching the conductor spacer bars to locate the conductor position and calculate the gallop offset. Reference [12] reported a method that captures each frame of images from the video and selects the split wire spacer as the feature for edge detection. By automatically searching for and locating the contour position of the spacer in each frame image, the center coordinates of the spacer, and the horizontal axis of the spacer, a he time series of the instantaneous displacement and displacement in the vertical axis direction is calculated. Finally, the main frequency and amplitude of conductor galloping are obtained by spectrum analysis. The method in reference [13] first extracts the spacer bars from the image using image matching and morphological operations, corrects for perspective distortion for skeleton extraction, and finally uses weighted invariant moment values for shape metrics. Several of the above methods using image processing techniques for conducting galloping monitoring suffer from low recognition accuracy in dim light or rain and fog. The method described in reference [14] uses microwave interference technology to obtain the parameters of the tower deformation, predicts the amplitude of the conductor galloping with microwave interference technology by affecting the coefficient of deformation factors, and uses the image fitting method to improve the microwave interference technology to predict and analyze the deformation of the tower. However, this method relies on manual measurement, and the degree of automation is not high. In addition, the wire galloping amplitude is predicted by the deformation of the tower, and there is a certain prediction error. Other studies in the literature focus on data collected on conductor galloping for risk prediction [15–17].

The second approach is based on the monitoring methods of acceleration transducers, an inertial navigation system (INS), and Beidou. The acceleration transducer [18,19], INS, Beidou [20–22], and other modules are installed on the conductor to collect the motion parameters of the conductor and calculate the characteristic amplitude of conductor galloping.

The second method is now the mainstream technology, but it has the following problems:

- Power supply problem. Since most UHV and EHV lines are DC lines that cannot be induced to receive power, modules such as acceleration sensors are powered by solar panels and batteries, which increase the load on the wires. At the same time, it is difficult for the limited battery capacity to support the high power consumption due to real-time detection by the monitoring module. In addition, dust on the solar panels and the degradation of battery energy storage performance will prevent the method from effectively monitoring conditions for extended periods.
- Security risks. Installation of detection modules on the wires not only increases the burden on the wires, but also these "active" devices will affect the electrical performance and safety of the wires, which is an additional safety hazard.
- The price is high. The acceleration sensor, inertial navigation, and especially the Beidou positioning module, also need to be equipped with data transmitters, Beidou

reference stations, wireless transmission modules, high-energy batteries, etc. The equipment costs are high, and the equipment must have strong electrical performance, electromagnetic compatibility, and protection performance. Hence, the equipment is expensive and difficult to popularize.

- Equipment maintenance is difficult. As the main equipment is installed on the wires, once the equipment fails, it needs to be replaced on the wires, which are usually operating online, presenting great difficulty and heavy work burdens for the power operation and maintenance departments.

Since there are many safety hazards with the contact types, this paper focuses on the non-contact monitoring method. Focusing on the problem with existing non-contact monitoring technology, namely, that of being affected by the light antenna, which causes the accuracy to decrease, a conductor galloping monitoring method based on the target detection of infrared sources is put forward. An infrared source label is installed on the conductor spacer as the detected target, a high-definition night vision infrared camera is installed on an electric power tower to take videos of the infrared source label, and the target recognition and tracking are carried out with an industrial personal computer (IPC), thus obtaining the motion trajectory of the infrared source label, and then calculating the characteristic amplitude of conductor galloping. In addition, the application of an infrared source label equips the system with monitoring functions for nighttime and foggy conditions.

3. Infrared Light Source Target Selection Algorithm

The system for a conductor galloping monitoring method based on target detection of an infrared source mainly comprises 3 parts: an infrared source label, high-definition night vision infrared camera, and IPC. Specifically, the infrared source label has remarkably morphological characteristics and reflects infrared light; the high-definition night vision infrared camera is used to take videos of the infrared source label; the IPC is used for target recognition and tracking of infrared source labels in the video shot by the high-definition night vision infrared camera, thus obtaining the motion trajectory of the infrared source label and then calculating the characteristic amplitude of conductor galloping. Taking advantage of the shortcomings of existing galloping monitoring methods, the improved design mainly includes the following:

- The application of infrared source labels and high-definition night vision infrared camera can ensure not only detection by the camera during the day, but also detection of conductor galloping at night or in damp and foggy environments.
- In view of the foggy condition in video scenes, a fast image defogging method combined with dark channel is adopted to enhance the image quality and the infrared source label recognition rate [23–26].
- As for possible defects and fractures of the infrared source label in binarized images, the algorithm for image corrosion and dilation is adopted to repair the shape of the infrared source [27,28].
- The low-power consumption system design and galloping emergency response design of the calculation unit reduce the operating power consumption of the system and ensure the calculation functionality [29–31].

3.1. System Framework

The system for the galloping monitoring method based on infrared light source target detection mainly consists of five parts: infrared light source label, high-definition night vision infrared camera, solution unit, solar panel and intranet platform, as shown in Figure 1.

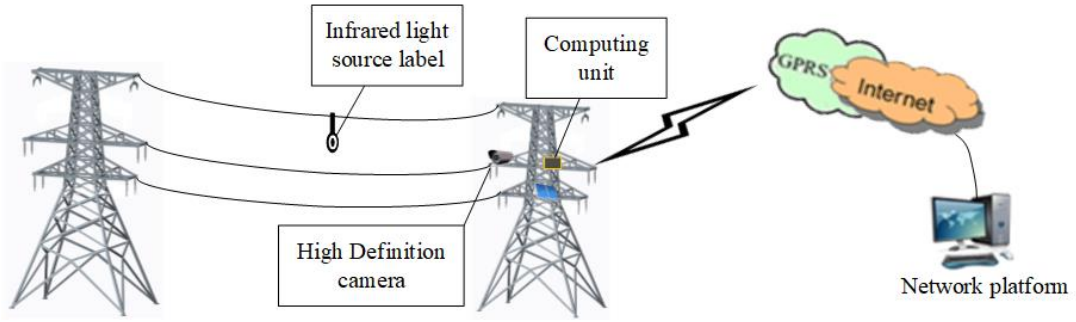

Figure 1. System framework diagram.

The infrared light source label has significant morphological characteristics and reflects infrared light. The high-definition night vision infrared camera is used to shoot video of the infrared light source label. The calculation unit used for the high-definition night vision infrared camera video of the infrared light source tags for target recognition and tracking, obtaining the trajectories of the infrared light source tag, and then calculating the characteristic magnitude of conductor galloping. Based on the national grid's "Q/GDW 242-2010 General technical specification for condition monitoring devices for transmission lines", the computed data are sent to the intranet platform. The solar panel draws power for the solver unit and high-definition night vision infrared camera. The internal network platform analyzes the data received on the conductor dancing features and issues dancing alarm references to power grid departments.

3.2. System Working Mode

The working mode of the system designed in this paper involves periodic collection and reporting and alarm and urgent reporting. By default, the system works every 40 min for 5 min. The dancing data are collected for calculation, and the data are packaged and sent to the cloud monitoring platform according to the specification formulated in Q/GDW 242-2010 General Technical Specification for Transmission Line Condition Monitoring Device. The system then sleeps for 35 min. If the solution unit detects an alarm notification of dancing features, it will continuously collect data and send them to the intranet platform. This working mode ensures that the solver can monitor the traversal effectively and maintain the low power consumption of the system.

For easy reference, all notations are described in Table 1.

Table 1. Description of notations.

Notation	Description
$H(x)$	foggy image with pixel x
$J(x)$	desired image after defogging
$t(x)$	transmittance
A	atmospheric optical intensity value
ρ	regulatory factor
$M(x)$	image composed of the minimum values in the three channels of image R, G and B containing fog
$M_{\text{ave}}(x)$	image produced by $M(x)$ average filter
m_{av}	mean of all elements in normalized $M(x)$
$src(x, y)$	grayscale value of each pixel of the grayscale image
M	threshold of binarization

Table 1. *Cont.*

Notation	Description
$dst(x, y)$	grayscale value of each pixel after binarization
R	rectangle filling rate
S_{area}	connected domain area
$S_{\text{rectangle}}$	minimum bounding rectangle area of connected domain
r	the ratio of rectangle length to width
$W_{\text{rectangle}}$	width of minimum bounding rectangle
$L_{\text{rectangle}}$	length of minimum bounding rectangle
(x_{ini}, y_{ini})	central coordinate of the infrared source
$(\overline{x}, \overline{y})$	the central coordinate of all infrared sources in the current frame image
len	conductor galloping amplitude
α	spatial mapping coefficient
d_{target}	the actual distance that the central coordinate of the infrared source moves
n_{pixel}	the number of pixels in the image that the distance of the central coordinate of the infrared source moves
θ	galloping ellipse inclination angle
E_r	relative error
d_{real}	the actual distance by gyroscope

3.3. Image Preprocessing

The image is modeled by the following fog pattern:

$$H(x) = J(x)t(x) + A(1 - t(x)) \tag{1}$$

where $H(x)$ is the existing image with fog, $J(x)$ is the desired image after defogging, A is the atmospheric optical intensity value, an empirical value that can be determined in advance, and $t(x)$ is the transmittance. Let $L(x) = A(1 - t(x))$, which is an ambient photon parameter; when the fog on the screen is severe, the smaller the transmittance $t(x)$, the greater the value $L(x)$. Therefore, the defogged image can be conveyed as:

$$J(x) = \frac{H(x) - L(x)}{1 - \frac{L(x)}{A}} \tag{2}$$

$L(x)$ is calculated as follows:

$$L(x) = \min\{\, [\min(\rho \times m_{av}, 0.9) \times M_{ave}(x)], \quad M(x)\,\} \tag{3}$$

where ρ is the regulatory factor, and the larger ρ is, the darker the overall picture is. $M(x)$ is the image composed of the minimum values in the three channels of image R, G and B containing fog, that is, $M(x) = \min_{c \in \{r,g,b\}} (H^c(x))$. $M_{\text{ave}}(x)$ is the image produced by $M(x)$ average filter, that is, $M_{ave}(x) = average(M(x))$; m_{av} is the mean of all elements in normalized $M(x)$. The value of $L(x)$ is the result of further reduction in the filtered value of $M(x)$.

As can be seen from Formula (3), $L(x)$ can be calculated by using the fast image defogging method combined with dark channel prior. It can not only ensure the effectiveness of defogging, but also avoid the problem of darkened images after defogging.

The image is transformed from the RGB chromaticity diagram to the GRAY grayscale image with a grayscale range of 0–255. The grayscale image is processed by median filtering

to eliminate noise interference, and the grayscale image is binarized. The formula is shown as (4):

$$dst(x,y) = \begin{cases} 255 & if \quad src(x,y) > M \\ 0 & otherwise \end{cases} \tag{4}$$

where $src(x,y)$ is the grayscale value of each pixel of the grayscale image, with a value range of 0–255; M is the threshold of binarization, and the appropriate value can be determined by experiment; $dst(x,y)$ is the grayscale value of each pixel after binarization, with a value of 0 or 255. Because the infrared source is a white circle in the image, the contour of the infrared source is clear, and the shape is clear after binarization. Moreover, most of the dark background in the image turns black, highlighting the shape of the infrared source.

3.4. Identification of the Calculation Central Coordinates of Infrared Source

As for possible defects and fractures of the infrared source in the binarized image, the algorithm of image corrosion and dilation is adopted to repair the shape of the infrared source.

The set of detected image contour points is stored in an array; each array represents a contour, and the closed region contained in each contour is called a connected domain. The perimeter of the connected domain refers to the number of pixels contained in the peripheral contour of the connected domain, and the area of the connected domain refers to the number of all pixels in the whole connected domain. Connected domains that are not within the minimum and maximum values of the perimeter and area are excluded.

The minimum bounding rectangle of each connected domain is drawn, and the infrared source is identified by using the geometric characteristics of the connected domain and its minimum bounding rectangle. Here, two characteristics of rectangle filling rate and the ratio of rectangle length to width are mainly used. The rectangle filling rate is the ratio of the above connected domain area to its minimum bounding rectangle area, and its formula is shown as (5):

$$R = S_{area} / S_{\text{rectangle}} \tag{5}$$

In Formula (5), R represents the rectangle filling rate, S_{area} is the connected domain area, and $S_{\text{rectangle}}$ is the minimum bounding rectangle area of the connected domain. The ratio of rectangle length to width is the ratio of minimum bounding rectangle length to width of the above connected domain, and its formula is shown as (6):

$$r = W_{\text{rectangle}} / L_{\text{rectangle}} \tag{6}$$

In Formula (6), r represents the ratio of rectangle length to width, $W_{\text{rectangle}}$ is the width of minimum bounding rectangle, and $L_{\text{rectangle}}$ is the length of minimum bounding rectangle. For instance, the infrared source is a circle, and the ratio of rectangle length to width of the circle is 1. An interval near 1 is set to exclude the connected domains in which the ratio of rectangle length to width is not in the interval. Each connected domain in the image is traversed, and the rectangle filling rate R and the ratio of rectangle length to width r are used to judge and screen, and the connected domains that meet both conditions are retained and identified as the infrared source. The center of the minimum bounding rectangle identified as the connected domain of the infrared source is taken as the center of the infrared source. Assuming that infrared sources are identified in the image of the current frame, their central coordinate takes the central coordinate (x, y) of all infrared sources in the current frame image as the final central coordinate of the infrared source in the current frame image, denoted as $(\overline{x}, \overline{y})$.

3.5. Calculation of Conductor Galloping Amplitude

Taking the central coordinate (x_{ini}, y_{ini}) of the infrared source in the static state of the conductor as the benchmark for monitoring, the displacement of the infrared source in the current frame image is calculated as the conductor galloping amplitude; its dancing trajectory is shown in Figure 2.

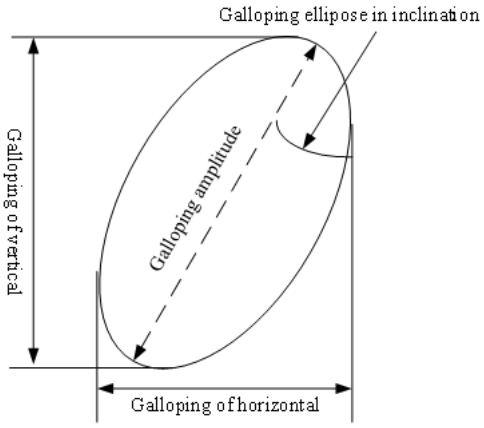

Figure 2. The galloping trace.

The formula is shown as (7):

$$len = 2 \times \alpha \times \sqrt{(\overline{x} - x_{ini})^2 + (\overline{y} - y_{ini})^2} \tag{7}$$

where *len* is the conductor galloping amplitude in the current frame image. α is the spatial mapping coefficient, which represents the actual spatial distance corresponding to a pixel in the image, and can also be calculated by offline calibration, and the formula is shown as (8).

$$\alpha = d_{\text{target}} / n_{pixel} \tag{8}$$

where d_{target} is the actual distance that the central coordinate of the infrared source moves, and n_{pixel} is the number of pixels in the image that the distance of the central coordinate of the infrared source moves. The above method for calculating the spatial mapping coefficient α is also applicable when the focal length of the camera changes.

3.6. Calculation of the Galloping Ellipse Inclination Angle and Galloping Frequency of the Conductor

Based on Figure 2 above, it is obtained that

$$\theta = \arctan(|\overline{x} - x_{ini}| / |\overline{y} - y_{ini}|) \tag{9}$$

In Formula (9), θ is the galloping ellipse inclination angle, the $|\overline{x} - x_{ini}|$ and $|\overline{y} - y_{ini}|$ are the half range of the horizontal and vertical galloping amplitudes, respectively. The conductor galloping frequency can be obtained by applying the fast Fourier transform to the galloping amplitude *len* of the morphological label of all obtained infrared sources.

4. Design of Hardware and Software

4.1. Design of Infrared Source Label

The infrared source label occupies a vital position in monitoring conductor galloping that directly determines the effectiveness and efficiency of galloping monitoring. Its design and installation are shown in Figure 3.

The morphological label of the infrared source uses a black acrylic board as the substrate; a white acrylic board in the shape of a concentric circle is embedded on the substrate, and a layer of infrared reflective film is affixed on the white acrylic board. During normal daytime conditions, high-definition night vision infrared cameras detect conductor galloping by detecting the contour features of white concentric circles. At night or in foggy conditions, the high-definition night vision infrared camera turns on the infrared light, and the light is reflected by the infrared source label, which gives the imaging of the infrared source in the camera remarkable characteristics. Moreover, the detection of the IPC is the same as in the normal daytime, and even better than that during normal daytime.

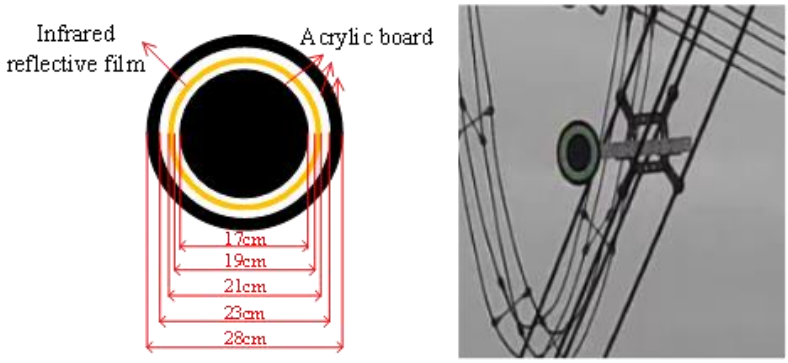

Figure 3. The infrared source label.

4.2. Design of the Calculation Unit

The solution unit consists of two parts: calculation unit and decision-making unit. Its hardware block diagram is shown in Figure 4.

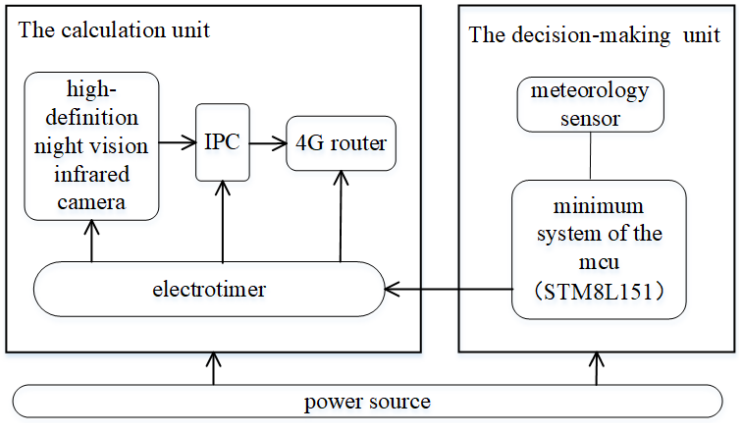

Figure 4. The structure of the hardware.

The calculation unit is composed of a high-definition night vision infrared camera, industrial personal computer, 4G router and electro timer. The high-definition night vision infrared camera is a fully automatic ball machine, with a focal length of 23 × 16 times; it has an efficient infrared array and low-power consumption circuit design, an irradiation distance of up to 200 m, and a built-in heat treatment device to prevent the ball machine from being covered with fog. The IPC has a 64-bit processor; Intel I7-5500U CPU with main operating frequency of 2.4 GHz, and dual network ports, and supports power-on self-start. Network port 1 of the IPC interacts with the high-definition night vision infrared camera, and network port 2 connects to a 4G router. The 4G router supports TDD-LTE and FDD-LTE modes with transmission speeds of up to 150 Mbps and a timing relay using the RS485 communication interface.

The decision-making unit is composed of a minimum system with an MCU and weather station. The minimum system consists of an STM8L151 microprocessor, crystal oscillation circuit, reset circuit, and download circuit. The MCU minimum system and peripherals adopt 485-level communication mode; a MAX485 level conversion chip is selected, its serial port 1 is used for data interaction with the timing relay; the baud rate is 9600 bps and 8 data bits with no check bit. Its serial port 2 is used for data interaction with the weather station with a baud rate of 9600 bps, 8 data bits, and even parity check. The weather station can measure temperature, humidity, wind speed, and wind direction using the 485-interface output.

The power supply circuit can convert the solar panel input voltage of 18V into multiple voltage outputs: a 3.3 V power supply for the microcontroller minimum system; 5 V

to power the weather station; and 12 V to power the 4G routers, industrial computers, and relays.

4.3. Work Flow of The Calculation Unit

The work flow chart of the calculation unit is shown in Figure 5. In the working mode, the processor is connected to the high-definition night vision infrared camera through network interface 1 to ensure the speed of video transmission. The power supply for the camera and IPC is controlled by a timing relay, and the calculation unit works for 5 min every 40 min by setting a timer. In the working mode, after the start and initialization of the galloping monitoring unit, calculation of the characteristic amplitude of the galloping begins, then stops after 5 min.

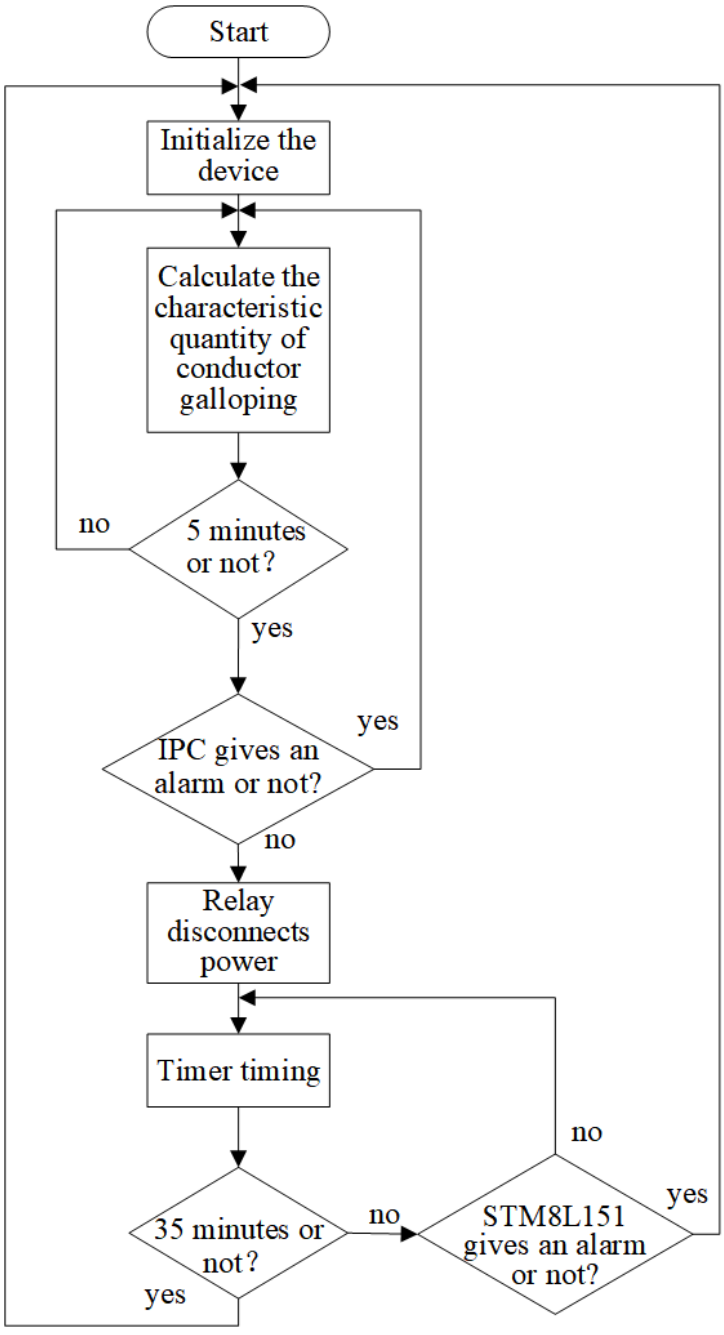

Figure 5. The calculation unit.

The IPC judges whether the characteristic amplitude of the galloping warrants an alarm or not. If the alarm is given, the system will continue to work. If the alarm is not given, the timing relay disconnects the power supply and starts the timer for 35 min. Within 35 min, if the STM8L151 single-chip microcomputer detects that the meteorological data has given an alarm, the timing relay controlled by serial interface 1 will turn on the power supply of the camera and IPC to allow them to directly enter working mode and increase the detection frequency. Within 35 min, if the STM8L151 single-chip microcomputer does not give an alarm, after 35 min, the galloping monitoring unit will also enter the working mode.

4.4. Cost Estimation

The system consists of infrared light source tags, high-definition night market infrared cameras, back-end calculation units and front-end display platforms. Both traditional image processing for non-contact monitoring and sensor-based contact monitoring technologies, back-end calculation units and front-end display platforms are essential. The only cost difference between the methods proposed in this paper is associated with the HD night vision infrared camera. This system uses a 2-megapixel infrared camera of the iDS-2DF8253I5X series (C) (DJ), and the cost is RMB 2500, which is equivalent to USD 400. Similar to the cost of other image processing methods, it is far lower than the Beidou monitoring technology that costs more than 25,000 yuan. Therefore, the monitoring method adopted in this paper has practical promotion value in engineering applications.

5. Testing and Data Analysis

5.1. Experimental Verification

In order to verify the effectiveness of the conductor galloping monitoring method based on infrared light source target detection, a series of experimental tests were carried out. We selected a 2-megapixel infrared camera with model iDS-2DF8253I5X series (C) (DJ) and a web-side software platform written in C++ language running on the Windows 2012 Server system to display the calculated conductor galloping data. Two iron tower models were selected, and the distance between them was 3 m. A thick rope was tied on the top of the two iron towers and the morphological label of the infrared light source was placed at the sag point of the rope, as shown in Figure 6.

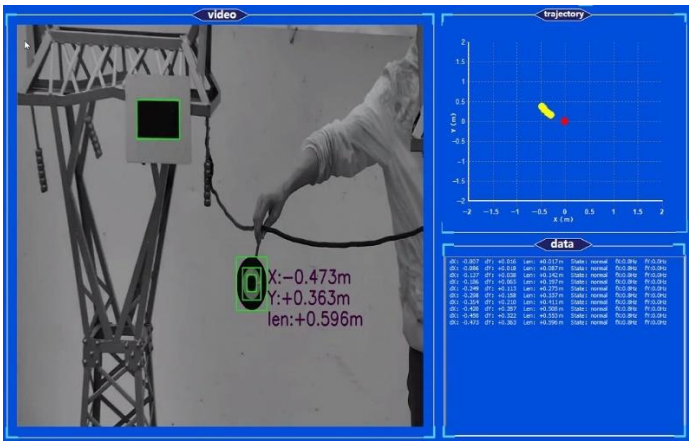

Figure 6. The galloping accuracy testing method.

In accordance with the results of the calculation unit, the actual offset and the measured offset in the horizontal and vertical directions were compared, as shown in Tables 2–5. It can be seen from these figures that the deviation between the two was very small. When the distance was 200 m, the error between the two was 1.2%, which provided high detection accuracy and was able to meet the monitoring requirements of the power grid platform.

Table 2. Tag recognition performance at 50 m.

Actual Value (m)	Horizon (m)		Vertical (m)	
	Measured	Error	Measured	Error
1	1.003	0.003	1.004	0.004
1.5	1.503	0.002	1.5015	0.001
2	1.994	−0.003	1.994	−0.003
2.5	2.5025	0.001	2.51	0.004
3	3.009	0.003	3.003	0.001

Table 3. Tag recognition performance at 100 m.

Actual Value (m)	Horizon (m)		Vertical (m)	
	Measured	Error	Measured	Error
1	1.003	0.003	1.002	0.002
1.5	1.494	−0.004	1.506	0.004
2	2.004	0.002	1.994	−0.003
2.5	2.4925	−0.003	2.51	0.004
3	3.003	0.001	3.015	0.005

Table 4. Tag recognition performance at 150 m.

Actual Value (m)	Horizon (m)		Vertical (m)	
	Measured	Error	Measured	Error
1	1.006	0.006	0.995	−0.005
1.5	1.488	−0.008	1.5105	0.007
2	2.014	0.007	2.012	0.006
2.5	2.4775	−0.009	2.4875	−0.005
3	3.018	0.006	3.018	0.006

Table 5. Tag recognition performance at 200 m.

Actual Value (m)	Horizon (m)		Vertical (m)	
	Measured	Error	Measured	Error
1	1.009	0.009	0.989	−0.011
1.5	1.4775	−0.015	1.518	0.012
2	2.026	0.013	1.974	−0.013
2.5	2.4725	−0.011	2.5325	0.013
3	3.036	0.012	3.033	0.011

5.2. Application Test

The system was installed on an 800 kV UHV transmission line in Xuancheng city, Anhui Province in November 2019. The morphology label of the infrared light source was installed on the spacer bar near the sag point of the wire, the solution unit was installed on the first-level platform of the pole tower, the solar panel and solution unit were fixed on the pole tower in the form of a hoop, and the camera was installed in a customized fixed structure, as shown in Figure 7. In Figure 7, the yellow circle represents the infrared light source label.

Figure 7. The installation of infrared light tag.

The recognition performance on foggy days is as shown in Figure 8; the solver could still detect the infrared light source effectively. Under the strong support of Anhui Power Transmission and Transformation Engineering Co., Ltd. (Hefei, China), the detection accuracy of this system has been compared in several groups of tests. At the spacer bar where the label is mounted, a gyroscope was also installed. Over a short period of time, the gyroscope still had high detection accuracy. The gyroscope transmitted the dancing data on the detected wire to the main monitoring station through wireless mode.

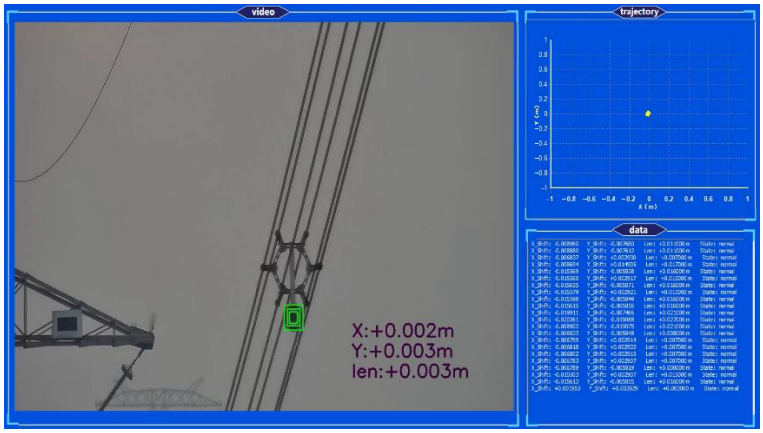

Figure 8. The recognition performance on foggy days.

Galloping test experiments were carried out on the methods in this paper to record the different positions of the wire galloping and to restore the spatial movement trajectory based on the measured horizontal and vertical data. At the spacer where the label was installed, a gyroscope was also installed to compare the gyroscope data with the data measured by the system. In the two groups of experiments shown in Figure 9, the orange trajectory represents the infrared light source method, the blue trajectory represents the monitoring results from the gyroscope, the horizontal axis represents the amplitude in the horizontal direction, and the vertical axis represents the amplitude in the vertical direction. According to the measured horizontal and vertical data, the spatial motion trajectory was restored, as shown in Figure 9. The data obtained with the method in this paper were basically equivalent to the data measured by the gyroscope, which can effectively monitor wire galloping.

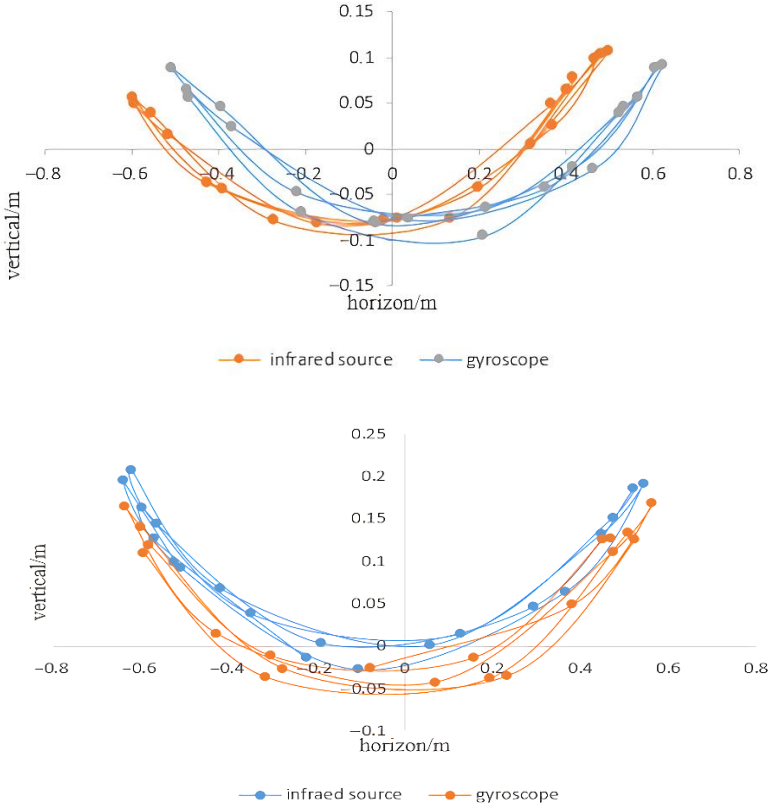

Figure 9. Comparison of experimental trajectories between the two groups.

To verify the effectiveness of the method in this paper, the experiment also compared it with two other methods, described in [12,14]. The infrared light source high-definition camera was set up at a distance of 400 m from the wire, and the other method devices similarly set up at a distance of 400 m. Taking the amplitude measured by the gyroscope as the reference standard, the method in this paper was compared with the amplitude measured by the other two methods, and the measurement accuracy was measured by the relative error. The relative error calculation formula is shown in Formula (10):

$$\mathrm{E_r} = \frac{d_{\mathrm{target}} - d_{real}}{d_{real}} \times 100\% \tag{10}$$

where d_{target} is the dance amplitude measured by the different methods. d_{real} is the dance amplitude measured with the gyroscope.

Figure 10 is a comparison of the relative errors of the measured amplitudes of the three methods. It can be seen that the relative error of the infrared light source was relatively small and basically about 3%, which did not change with time. This was because the infrared light source label was installed on the wire spacer and the high-definition night vision camera was installed on the tower. The infrared camera was capable of high-precision identification in dark and foggy conditions. The video monitor captured galloping images directly from the video, and the relative error at night and in foggy weather was large, reaching 10%~15%. The microwave interference technology used manual measurements, and the degree of automation was not high. Second, it predicted the galloping amplitude of the wire through the deformation of the tower. The accuracy was not high enough, and the relative error was 5% to 10%.

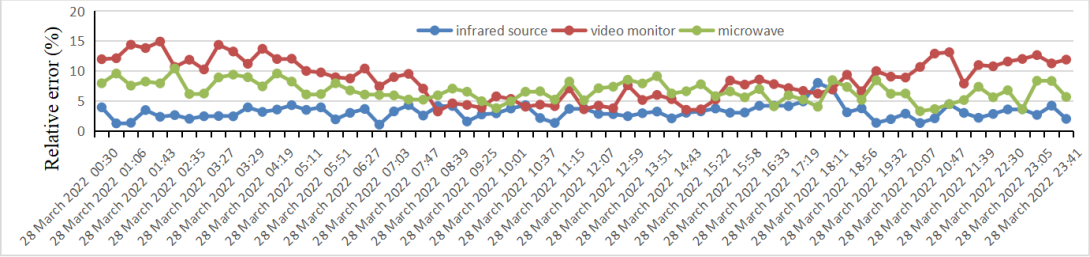

Figure 10. Relative errors of three monitoring methods in measuring amplitude.

6. Conclusions

A conductor galloping monitoring method with high recognition and good detection accuracy based on the target detection of an infrared source was proposed. The calculation unit adopts periodic acquisition and alarm acquisition, which not only ensures the effectiveness of system detection and low power consumption by system operations, but also enables the device to run stably for long periods to cope with bad meteorological conditions. Compared with the monitoring technology of INS and Beidou positioning, this system does not directly contact the live conductors, is thus safe and reliable with no potential electrical hazards or remarkable morphological characteristics, and costs less. Compared to other image processing monitoring methods, this system is unaffected by changes in weather and lighting, and offers high monitoring accuracy at no additional cost. The experimental data indicate that the method has high detection accuracy and can be applied in the automatic monitoring of conductor safety in the State Grid.

Author Contributions: Conceptualization, Y.G. and J.Y.; formal analysis, Y.G., H.P. and K.Z.; investigation, J.Y., Y.W. and N.X.; writing—original draft, Y.W., H.P., Y.G. and N.X; writing—review and editing, G.Y., Y.G., K.Z. and J.Y. All authors have read and agreed to the published version of the manuscript.

Funding: This research was funded by State Grid Co., Ltd. Headquarters Technology Project, grant number 5500-202140127A.

Data Availability Statement: All data have been included within the manuscript.

Acknowledgments: We would like to thank the people who helped us annotate the emotion labels of the dialogues in this study.

Conflicts of Interest: The authors declare no conflict of interest.

References

1. Chen, Z.G.; Li, H.Q.; Chen, Y.F. An Active Anti-Galloping Method and Device of Overhead Transmission Lines. Available online: https://patents.google.com/patent/CN101859993A/en (accessed on 13 October 2010).
2. Zhao, B.; Cheng, Y.F.; Wang, J.C. Theoretical analysis and counter measures on the galloping of iced overhead transmission lines in Hubei in early 2015. *J. Vib. Shock* **2017**, *36*, 93–97.
3. Yang, S.G.; Liu, X.H.; Liang, H.B.; Cai, M.Q. Galloping Characteristics of Iced Transmission Lines under the Excitation of Periodic Aerodynamic Loads. *Noise Vib. Control* **2021**, *41*, 1–8.
4. Zou, M.; Liu, X.H.; Cai, M.Q. Galloping Stability Analysis of Quad-bundled Conductors with Crescent Ice Covering Considering Wake Effect. *Noise Vib. Control* **2021**, *41*, 34–41.
5. Zheng, M.L.; Liu, J.; Deng, B. The Noether Symmetry and Conserved Quantity of Galloping Iced Power Transmission Lines. *Appl. Math. Mech.* **2021**, *42*, 275–281.
6. Min, C.G.; Liu, X.H.; Yan, B. The influence of method of multiple scales and averaging on the galloping characteristics of the crescent iced conductor. *Sci. Technol. Eng.* **2020**, *20*, 13206–13212.
7. Han, J.S.; Lv, H.P.; Li, D.Y. Prediction of Transmission Line Galloping Using Improved BP Neural Network Based on Genetic Algorithm. *Power Syst. Clean Energy* **2021**, *37*, 1–7.
8. Wang, T.; Wu, D.Z.; Hu, K. An algorithm based on complementary filtering to reshape galloping track of transmission line. *Comput. Meas. Control* **2017**, *21*, 173–176.
9. Liu, X.H.; Zhang, L.F.; Yan, B. Modal Analysis of Iced Conductor Galloping for Continuous Spans. *J. Syst. Simul.* **2016**, *28*, 2647–2654.

10. Nathan, P.; Georgios, F.; Kendric, O.; Meeko, O. A UAV-enabled Dynamic Multi-Target Tracking and Sensing Framework. In Proceedings of the 2020 IEEE Global Communications Conference (GLOBECOM 2020), Taipei, Taiwan, 7–11 December 2020.
11. Huang, X.B.; Zhang, Y.; Cheng, W.F. Galloping monitoring method of transmission line based on image matching. *High Volt. Eng.* **2014**, *40*, 808–813.
12. Yin, H.; Zhang, X.M.; Chen, X.X. Galloping Information Extraction and Spectral Analysis for Transmission Lines Based on Video Monitoring. *High Volt. Eng.* **2017**, *43*, 2889–2895.
13. Jin, L.J.; Hu, J.; Yan, S.J. Method of spacer fault diagnose on transmission line based on image processing. *High Volt. Eng.* **2013**, *39*, 1040–1045.
14. Hu, L.J.; Wu, R.; Huang, Y.J.; Ye, Z.R. Research on monitoring tower deformation and conductor galloping amplitude based on microwave interference technology. *China Meas. Test* **2022**, *48*, 129–135.
15. Wang, J.; Liu, Z.X.; Zhang, Q.W.; Chuan, A. Research on On-Line Monitoring of Transmission Tower Stress. *Appl. Mech. Materials* **2014**, *668–669*, 948–952. [CrossRef]
16. Sun, J.; Wu, C.Y.; Cheng, Y.F. Explainable AI Enabled Conductor Galloping Predictor Design. In Proceedings of the 2021 IEEE Power & Energy Society Innovative Smart Grid Technologies Conference (ISGT), Washington, DC, USA, 16–18 February 2021.
17. Wang, K.; Sun, J.; Wu, C.Y. Conductor Galloping Prediction on Imbalanced Datasets: SVM with Smart Sampling. In Proceedings of the 2020 IEEE Power & Energy Society General Meeting (PESGM), Montreal, QC, Canada, 2–6 August 2019.
18. Zhang, F.; Xiong, L.; Liu, Y. Transmission lines galloping monitoring system based on accelerometer sensors. *Electr. Meas. Instrum.* **2009**, *46*, 30–33.
19. Wang, Q.Z.; He, Y.G.; Deng, F.M. Online monitoring technology of transmission line galloping based on RFID acceleration sensor tags. *Transducer Microsyst. Technol.* **2017**, *36*, 99–102.
20. Hu, Z.J.; Li, H.J.; Wen, S.H. Online monitoring of transmission conductor wave and wind gallop based on differential GPS. *Electr. Power Autom. Equip.* **2012**, *32*, 120–124.
21. Feng, W.B.; Guo, T.; Yang, H.M. Galloping characteristics analysis and monitoring system of continuous crescent iced conductor. *Chin. J. Appl. Mech.* **2021**, *38*, 2188–2195.
22. Huang, X.B.; Zhao, L.; Chen, G.M. Design of a Wireless Sensor Module for Monitoring Conductor Galloping of Transmission Lines. *Sensors* **2016**, *16*, 1657. [CrossRef]
23. Du, Z.L.; Shi, Y.; Li, X.L. An image dehazing algorithm based on atmospheric difference. *J. Terahertz Sci. Electron. Inf. Technol.* **2019**, *17*, 1078–1085.
24. Fu, H.; Wu, B.; Li, L.F. Definition Recovery of Haze Image Based on Dark Channel Prior. *Comput. Eng.* **2016**, *42*, 232–237.
25. Huang, F.Y.; Li, G.; Zou, C.F. Adaptive image dehanzing based on dark channel prior. *J. Optoelectron.·Laser* **2019**, *30*, 1323–1330.
26. Liu, J.P.; Yang, Y.W.; Wei, G. Noise Reduction of Chaotic Signals Based on Phase Space Reconstruction and Singular Spectrum Analysis. *J. South China Univ. Technol. (Nat. Sci. Ed.).* **2018**, *46*, 86–91.
27. Du, H.M.; Jiang, B.B.; Chang, L.B. Improvement and parallel implementation of dilation and erosion algorithms. *J. Xi'an Univ. Posts Telecommun.* **2017**, *22*, 88–93.
28. Deng, S.H.; Huang, Y. Fast algorithm of dilation and erosion for binary image. *Comput. Eng. Appl.* **2017**, *53*, 207–211.
29. Wang, Z.L.; Zhao, X.F.; Wu, G.L. Design and realization of micro-meteorological disaster monitoring and pre-warning system in power grid. *Power Energy* **2014**, *35*, 712–716.
30. Wang, J.; Tan, R.H. Design of ultra-low power infrared optical communication system based on embedded technology. *Laser J.* **2020**, *41*, 177–181.
31. Chen, S.T.; Xie, W.B.; You, Y.M. The design of infrared and utrasonic rangefinder based on STM8. *Embed. Technol.* **2011**, *37*, 32–34.